Disordered porous solids : from chord distributions to small angle scattering

P. Levitz, D. Tchoubar

Classification
Physics Abstracts
61.10D — 61.12D — 61.40

Disordered porous solids : from chord distributions to small angle scattering

P. Levitz and D. Tchoubar

Centre de Recherche sur la Matière Divisée, CNRS, 1B rue de la Ferollerie, 45071 Orléans, France

(*Received 4 March 1992, accepted 16 March 1992*)

Résumé. — Les solides poreux biphasiques sont des exemples de milieux interfaciaux complexes. La diffusion aux petits angles (SAS) dépend fortement des propriétés géométriques de l'interface partitionant le milieu poreux. Les propriétés de la dérivée seconde de la fonction d'autocorrélation de densité définit quantitativement le niveau de connection entre la diffusion aux petits angles et les caractéristiques statistiques de cette interface. Une expression utilisable de cette seconde dérivée, impliquant les distributions de cordes associées à la phase massique et au réseau de pores, fut proposée par Mering et Tchoubar (MT). Mettant à profit la possibilité actuelle d'une comparaison quantitative entre les techniques d'imagerie et la diffusion aux petits angles, ce papier tente de compléter et d'étendre l'approche MT. Dans un premier temps, nous montrons en quoi la connaissance de ces distributions de cordes permet de distinguer certains types de désordres structuraux. Une relation explicite entre le spectre de diffusion aux petits angles et les distributions de cordes est alors proposée. Dans une troisième partie, l'application à différents types de désordre est discutée et les prédictions du modèle comparées aux résultats expérimentaux disponibles. Par utilisation du traitement d'images, nous nous intéressons à trois types de désordre : le milieu aléatoire de Debye, pour ses propriétés à grandes distances, le désordre « corrélé » avec une attention particulière pour le cas d'un verre poreux (le Vycor) et enfin des organisations complexes où des propriétés d'invariance d'échelle de longueur peuvent être observées.

Abstract. — Disordered biphasic porous solids are examples of complex interfacial media. Small angle scattering strongly depends on the geometrical properties of the internal surface partitioning a porous system. Properties of the second derivative of the bulk autocorrelation function quantitatively defines the level of connection between the small angle scattering and the statistical properties of this interface. A tractable expression of this second derivative, involving the pore and the mass chord distribution functions, was proposed by Mering and Tchoubar (MT). Based on the present possibility to make a quantitative connection between imaging techniques and the small angle scattering, this paper tries to complete and to extend the MT approach. We first discuss how chord distribution functions can be used as fingerprints of the structural disorder. An explicit relation between the small angle scattering and these chord distributions is then proposed. In a third part, the application to different types of disorder is critically discussed and predictions are compared to available experimental data. Using image processing, we will consider three types of disorder : the long-range Debye randomness, the « correlated » disorder with a special emphasis on the structure of a porous glass (the vycor), and, finally, complex structures where length scale invariance properties can be observed.

1. Introduction.

Disordered porous solids play an important role in industrial processes such as separation science, heterogeneous catalysis, oil recovery, glass and ceramic processings [1]. The confinement and the geometrical disorder of these systems strongly influence the dynamic or thermodynamic processes which can take place inside the pore network [2]. This raises the challenging problem of describing the morphology of these porous solids. A structural analysis can be handled using a number of techniques [3] : direct observation of the mass distribution by optical or electron microscopy, molecular adsorption, direct energy transfer. Correlations at different length scales of the mass distribution are generally probed by small angle scattering (SAS). It is well known that the density fluctuations are the main origin of the scattering. In the case of a biphasic matrix, these fluctuations are localized just at the sharp interface which partitions the system. The small-angle scattering, considered as a purely interfacial phenomenon [4], is then strongly dependent on the geometrical properties of this oriented interface. This statement can be qualitatively understood if we consider a disordered porous medium as completely defined either by its mass distribution or by the oriented interface separating the « void » space from the « mass » part of the matrix. Properties of the second derivative of the mass autocorrelation function quantitatively define the level of connection between small-angle scattering and the statistical properties of the interface [5, 6]. This has been known for a long time, almost for smooth and convex particles. As shown by Guinier [7] and Porod [8], a relationship between the shape of a convex particle and its scattering can be made using the concept of chord distribution. A chord is a segment belonging to the particle and having both ends on the interface. It can be considered as a linear path which correlates two distinct points of the interface. Many attempts have been made to develop this concept further. Connections between small r expansion of the chord distribution and local or semi-local properties of the interface such as the curvature, the angularity were developed independently by Porod [8], Mering and Tchoubar [9], Wu and Schmidt [10, 11]. These different studies were essentially dealing with convex particles where only one chord distribution was needed. Extension to a biphasic porous solid (generally a non-convex structure) is more complicated. The general expression of the second derivative of the mass autocorrelation function involves a « delicate » surface integral, as shown by Ciccarillo *et al.* [5]. Mering and Tchoubar [12] have proposed a more tractable expression of this second derivative, involving the « pore » and « mass » chord distribution functions. Several hypotheses are involved in their analysis : (i) the porous solid is considered as an isotropic biphasic random media ; (ii) their derivation considers the distribution of matter along a random line (an one-dimensional analysis) ; (iii) a specific type of randomness where uncorrelation between adjacent chords has to be assumed. At this time, in the sixties, no attempt was made to give an explicit expression of the small angle scattering involving chord distribution functions and able to be checked by independent experimental data. Based on the present possibility to make a quantitative connection between imaging techniques and small-angle scattering, this paper tries to complete and extend the approach of Mering and Tchoubar. In section 2, we discuss how chord distribution functions can be used as fingerprints of the structural disorder. As examples, we give analytical expressions and large r expansions of chord distribution functions for two types of random binary media : (i) the Debye randomness and (ii) systems where a length scale invariance property can be observed either for the bulk part or the interface. In section 3, the second derivative of the mass autocorrelation, involving the « pore » and « mass » chord distributions, is computed using a « three-dimensional » derivation. We also give an explicit expression of the small-angle scattering which directly depends on the Fourier transforms of chord distributions. In part 4,

the application to different types of randomness is critically discussed and predictions are compared to available experimental data. Using image processing, we will consider three types of disorder : the long-range Debye randomness, « correlated » disorder with a special emphasis on the structure of the vycor porous glass, and, finally, complex structures where length scale invariance properties can be observed.

2. Biphasic random medium and chord distribution functions.

2.1 BACKGROUND. — A simple description of a two-phase system includes two assumptions. First, each phase is considered as homogeneous and is characterized by its average density. Second, these two phases are separated by an ideal sharp interface. As discussed by Ciccariello [13], the real structure is then probed with a coarse grain size larger than the atomic scale. In this domain of approximation, it is possible to define at least two types of chord distribution functions [14]. The chord size distribution « in number » (called for short : chord distribution) is related to the conditional probability of having a chord size between r and $r + dr$, knowing that the chord begins at a specific point of the interface. This distribution will be noted $f_p(r)$ or $f_m(r)$ where the indices p and m stand for pore and mass, respectively. The chord size distribution « in length » $g_p(r)$ ($g_m(r)$) gives the probability density to find a pore (mass) chord having a size between r and $r + dr$ and passing through a point M randomly distributed in the pore (mass) phase. These distributions are null for negative distances. The relation between g and f distributions is [12, 14] :

$$g_i(r) = \frac{r f_i(r)}{\bar{r}_i} \qquad i = \mathrm{m}, \mathrm{p} \tag{1}$$

with

$$\bar{r}_i = \int_0^\infty r f_i(r)\, dr \tag{2}$$

and

$$\int_0^\infty f_i(r)\, dr = 1 . \tag{3}$$

An interesting question can be asked at this level, concerning the possibility of using chord distribution functions as fingerprints of different models of disorder. In the next two sections, we discuss two of them : Debye randomness and disorder involving a length scale invariance.

2.2 DEBYE RANDOMNESS. — A theory of small-angle scattering from a biphasic random system was first proposed by Debye, Anderson and Brumberger [15, 16]. As recently discussed by Ciccariello [17], randomness in Debye's sense is related to the theory of stationary random functions [18]. More particularly, a « lineal » analysis of a Debye random system is closely connected with the model of the random telegraph signal solved by Rice [19]. Let $Q_i(r)$ denote the probability that no collision with the interface occurs along a segment of length r starting from a random point M located either in the pore (i = p) or in the mass phase (i = m). Assuming a Debye random system, the probability that no collision occurs in the interval of length $r + dr$ reads as :

$$Q_i(r + dr) = Q_i(r)\,(1 - \mu_i\, dr) \qquad i = \mathrm{p}, \mathrm{m} . \tag{4}$$

In this equation, two hypotheses are implicitly assumed. First, any event occurring on one side of the random line going through M is independent of any events occurring on the other

side. Second, the probability densities, μ_p and μ_m, of hitting the interface from the pore or the mass part of the matrix are constant. The probability that the first crossing point appears in the interval $(r, r + dr)$ is written as :

$$P_i(r)\, dr = Q_i(r)\, \mu_i\, dr \qquad i = p, m . \tag{5}$$

Combining equations (4) and (5) we get :

$$P_i(r) = \mu_i \exp(-\mu_i r) \qquad i = p, m . \tag{6}$$

The chord size distribution functions in length are computed using the convolution of $P_i(r)$ with itself :

$$g_i(r) = \mu_i^2 \int_0^r \exp(-\mu_i (r - r_1)) \exp(-\mu_i r_1)\, dr_1 . \tag{7}$$

Using equation (1), the two chord size distribution functions in number read :

$$f_i(r) = \frac{1}{\bar{\ell}_i} \exp(-r/\bar{\ell}_i) \tag{8}$$

with

$$\bar{\ell}_i = 1/\mu_i . \tag{9}$$

As shown in section 3, equation (8) permits the retrieval of the exponential variation of the bulk autocorrelation and consequently the well known Debye expression for small-angle scattering [16]. However, the negative exponential form of $f_p(r)$ and $f_m(r)$ raises some questions concerning the local properties of the interface. For a completely smooth (differentiable) interface, the small r expansion of the two chord distributions scales as r. The positive slope of this linear relationship is directly related to the curvature properties of the interface [10, 20]. Debye randomness acts in a different way. Small r expansion of equation (8) exhibits a positive value at the origin and a negative slope. This type of disorder involves a strong interfacial angularity [5, 8, 9, 12]. This explains why the scattering intensity predicted by Debye does not follow the asymptotic behavior predicted by Kirste and Porod [21] for smooth and curved interfaces.

2.3 DISORDER INVOLVING A LENGTH SCALE INVARIANCE. — We consider disordered systems with length scale invariance properties. More specially, we will focus on the long-range behavior of chord distribution functions. Let us consider a biphasic medium having a self similar interface. The intersection of this surface with a random line is also a self similar set of points. Using the rule of thumb concerning intersection of sets [22], the number of intersection points along a distance R is :

$$N_S(R) = F_S\, R^{\bar{d}_S - 2} \tag{10}$$

where $\bar{d}_S$ is the fractal dimension of the interface and F_S, a shape factor. The average chord lengths for the pore (or the mass) portion of this matrix, computed on a characteristic size R, is given by :

$$(\bar{\ell}_i)_R \propto \frac{R \Phi_i(R)}{N_S(R)} \qquad i = m, p \tag{11}$$

where $\Phi_i(R)$ is the average volume fraction of the phase i, measured on the length scale R. From equation (2), we have

$$(\overline{l_i})_R = \int_0^R r f_i(r)\, dr \tag{12}$$

and the long range behavior of chord distribution functions can be written as :

$$f_i(R) \propto \frac{1}{R} \frac{d(\overline{l_i})_R)}{dR} \qquad i = m, p . \tag{13}$$

Let first consider the case of a matrix having a self similar surface and a compact (non-fractal) distribution of the mass and the pore networks [23]. $\Phi_m(R)$ and $\Phi_p(R)$ are independent of R and we get :

$$f_i(R) \propto \frac{1}{R^{\bar{d}_S - 1}} \qquad i = m, p . \tag{14}$$

A second interesting situation concerns a biphasic medium having a fractal distribution of mass as found, for instance, in diffusion limited aggregates, cluster-cluster structures [24]. In this case, the mass volume fraction scales with R as :

$$\Phi_m(R) = F_m\, R^{(\bar{d}_m - 3)} \tag{15}$$

and

$$\Phi_p(R) = 1 - \Phi_m(R) \tag{16}$$

where F_m is a shape factor. For a mass fractal, the two exponents $\bar{d}_m$ and $\bar{d}_S$ are equal [23] and we obtain from equations (10) and (11) :

$$(\overline{l_m})_R = \frac{F_m}{F_S} \tag{17}$$

The average « mass » chord length is independent of the scale used in the computation. The mass chord distribution function has a well-defined first moment and must decay faster than $1/r^2$ to avoid a logarithmic divergence at large r. On the contrary, the pore chord distribution function scales as :

$$f_p(R) \propto \frac{1}{R^{\bar{d}_m - 1}} \tag{18}$$

In the three former examples, large r expansions of chord distribution functions exhibit specific properties of the structural disorder. It can be observed that equations (14) and (18) can be directly used on a random section of the matrix. In this case, the exponent, such as $(\bar{d}_S - 1)$, gives the fractal dimension of the intersection of the 3D interface and a random plane.

3. From chord distribution to small-angle scattering.

According to classical theory, the small angle scattering $I(\mathbf{q})$ is related to the 3D Fourier transform of the fluctuation autocorrelation function :

$$\eta^2(\mathbf{r}) = \frac{1}{V}\int d\mathbf{r}_0(\rho(\mathbf{r}_0) - \bar{\rho})\,(\rho(\mathbf{r}_0 + \mathbf{r}) - \bar{\rho}) \tag{19}$$

where $\rho(\mathbf{r})$ is the mass (the density) distribution and $\bar{\rho}$ the volume average of $\rho(\mathbf{r})$.

As mentioned in the introduction, small-angle scattering is strongly dependent on the geometrical properties of the interface separating the pore and the mass part of the matrix. Properties of the second derivative of the mass autocorrelation function quantitatively define the level of connection between small-angle scattering and the statistical properties of this interface [5]. For an isotopic biphasic random medium, an expression of this second derivative, involving the « pore » and « mass » chord distribution functions has been proposed [12]. This computation is based on a statistical analysis of the medium along a random line and gives, for $0 \leqslant r$:

$$\eta^2(r)'' = \frac{S_V}{4}\,(G(r) - 2\,\delta(r)) \tag{20}$$

with

$$G(r) = f_m(r) + f_p(r) - 2\,f_m(r) * f_p(r) + \\ + f_m(r) * f_p(r) * f_m(r) + f_p(r) * f_m(r) * f_p(r) - \cdot \tag{21}$$

The convolution product is symbolized by a star. S_V is the total interfacial area per volume unit. $G(r)$ is null for $r < 0$. The Dirac distribution on the rhs of equation (20) is directly connected with a finite discontinuity of $\eta^2(r)'$ at $r = 0$ (i.e. a finite value of S_V). This singular part of equation (20) determines the q^{-4} leading term in the high q expansion of the small angle scattering (The Porod law) and the linear behaviour of $\eta^2(r)$ at very small r.

The regular part of $\eta^2(r)''$, noted $[\eta^2(r)'']$ and equal to $S_V \cdot G(r)/4$, can be retrieved using a « three-dimensional » computation. Let us start from the functional expression proposed by Ciccariello *et al.* [5] :

$$[\eta^2(r)''] = -\frac{S_V}{4\pi}\left[\frac{1}{S}\int_S dS \int_{4\pi} d\hat{\boldsymbol{\omega}}(\boldsymbol{\sigma}_S \cdot \hat{\boldsymbol{\omega}}) \int_S dS'(\hat{\boldsymbol{\sigma}}_{S'} \cdot \hat{\boldsymbol{\omega}})\,\delta(\mathbf{r}_{SS'} - r\hat{\boldsymbol{\omega}})\right] \tag{22}$$

r is positive or null. S is the total surface. $\hat{\boldsymbol{\sigma}}_S$ is the unit vector perpendicular at the surface S in the point to which the differential element dS refers. $\hat{\boldsymbol{\sigma}}_S$ and $\hat{\boldsymbol{\sigma}}_{S'}$ lie outside the mass network. Equation (22) is mathematically significant if the boundary S is such that a tangent plane can be defined almost everywhere, except for a set of singular points having a null measure. Looking around a statistical point O_S belonging to the interface, the angular average over all possible directions $\hat{\boldsymbol{\omega}}$ can be split into two equal parts. The tangent plane to the surface, at O_S, defines two half spaces : one for directions pointing to the pore network (noted Ω^+), and one for solid angles pointing to the mass phase (noted Ω^-). Equation (22) can be written :

$$[\eta^2(r)''] = \frac{S_V}{4\pi}\,\langle F_+(O_S, r) + F_-(O_S, r)\rangle \tag{23}$$

with

$$F_{(\pm)}(O_S, r) = \int_{\Omega^{(\pm)}} d\hat{\boldsymbol{\omega}}(\hat{\boldsymbol{\sigma}}_S \cdot \hat{\boldsymbol{\omega}}) \int_S dS'(\hat{\boldsymbol{\sigma}}_{S'} \cdot \hat{\boldsymbol{\omega}})\,\delta(\mathbf{r}_{SS'} - r\hat{\boldsymbol{\omega}})\,. \tag{24}$$

The brackets stand for the total surface average, defined by the first integral in equation (22).

Let us consider a local orthogonal coordinate system specified by the tangent plane at the point O_S (x and y axis) and the direction $\hat{\sigma}_S$ (the z axis). Using standard differential geometry one gets :

$$dS'(\hat{\sigma}_{S'} \cdot \hat{\omega}) = d\theta' \, d\varphi' \, P(\theta', \varphi', \theta_\omega, \varphi_\omega) \tag{25}$$

and

$$\delta(\mathbf{r}_{SS'} - r\hat{\omega}) = \frac{1}{r^2 \sin(\theta_\omega)} \delta(\theta' - \theta_\omega) \, \delta(\varphi' - \varphi_\omega) \, \delta(r_{SS'} - r) \tag{26}$$

where $(r_{SS'}, \varphi', \theta')$ and $(\varphi_\omega, \theta_\omega)$ are the spherical coordinates of $O_{S'}$ and $\hat{\omega}$ respectively.

P is a lengthy function involving partial derivatives of $r_{SS'}$ with respect to θ' and φ'.

However for $\theta' = \theta_\omega$ and $\varphi' = \varphi_\omega$, we have :

$$P(\theta_\omega, \varphi_\omega, \theta_\omega, \varphi_\omega) = \mathrm{sgn}(\hat{\sigma}_{S'} \cdot \hat{\omega}) \, R_\omega^2 \sin(\theta_\omega) \, . \tag{27}$$

The second integral of equation (24) gives a series of contributions respectively associated with each intersection of the interface with a line having the direction $\hat{\omega}$. For Ω^+ half space, the first intersection from O_S involves a pore chord, the second a pore chord followed by a mass chord, and so on. Using equations (24), (26) and (27), we get :

$$F_+(O_S, r) = \int_{\Omega^+} d\hat{\omega}(\hat{\sigma}_S \cdot \hat{\omega}) \times$$
$$\times \left(-\frac{R^2_{\omega(p)}}{r^2} \delta(R_{\omega(p)} - r) + \frac{R^2_{\omega(p,m)}}{r^2} \delta(R_{\omega(p,m)} - r) - \frac{R^2_{\omega(p,m,p)}}{r^2} \delta(R_{\omega(p,m,p)} - r) + \cdot \right) \tag{28}$$

$R_{\omega(p)}$ is the length of the pore chord which goes from O_S to the first intersection along the direction $\hat{\omega}$. Related to the second intersection, $R_{\omega(p,m)}$ is the total length, along the direction $\hat{\omega}$, of the pore chord followed by a mass chord, and so on.

The next step consists in averaging equation (28) over all possible positions of O_S. There is no simple and general way of obtaining this average. If adjacent pore and mass chords are strongly correlated, the computation has to take into account distribution functions involving two, three,... consecutive chords. Following Mering and Tchoubar [12], we have to consider a specific type of randomness where statistical isotropy of the matrix and uncorrelation between adjacent chords are assumed. This is a strong hypothesis which must be checked for each system. in this case, we have :

$$\left\langle \int_{\Omega^+} d\hat{\omega}(\hat{\sigma}_S \cdot \hat{\omega}) \frac{R^2_{\omega(p)}}{r^2} \delta(R_{\omega(p)} - r) \right\rangle =$$
$$= \left(\int_0^{2\pi} d\varphi_\omega \int_0^{\pi/2} d\theta_\omega \sin(\theta_\omega) \cos(\theta_\omega) \right) \left(\int du f_p(u) \frac{u^2}{r^2} \delta(u - r) \right) = \pi f_p(r) \tag{29}$$

and

$$\left\langle \int_{\Omega^+} d\hat{\omega}(\hat{\sigma}_S . \hat{\omega}) \frac{R^2_{\omega(p,m)}}{r^2} \delta(R_{\omega(p,m)} - r) \right\rangle = \pi f_p(r) * f_m(r) \, . \tag{30}$$

Finally we get :

$$\langle F_+(O_S, r) \rangle = \pi(- f_p(r) + f_p(r) * f_m(r) - f_p(r) * f_m(r) * f_p(r) + \cdot \quad) \tag{31}$$

and

$$\langle F_{-}(O_S, r)\rangle = -\pi(+f_m(r) - f_m(r) * f_p(r) + f_m(r) * f_p(r) * f_m(r) - \cdot \quad) \tag{32}$$

$$[\eta^2(r)''] = \frac{S_V}{4}(f_m(r) + f_p(r) - 2 f_m(r) * f_p(r) + + f_m(r) * f_p(r) * f_m(r) + f_p(r) * f_m(r) * f_p(r) - \cdot \quad). \tag{33}$$

This result is similar to the regular part of equation (20).

Let us now try to connect the chord distribution functions to an explicit expression of the small-angle scattering, $I(q)$. For an isotropic medium we have :

$$I(q) = \int_0^\infty 4\pi r^2 \eta^2(r) \frac{\sin(qr)}{qr} \, dr \tag{34}$$

$\eta^2(r)$ being an even function, the former equation can be written :

$$I(q) = -\frac{2\pi}{q} \frac{d}{dq} (\text{Real}\ (\tilde{\eta}^2(q)) \tag{35}$$

with the general notation :

$$\tilde{w}(q) = \int_{-\infty}^{+\infty} w(r) \exp(iqr)\, dr \tag{36}$$

Using the standard properties of the Fourier transform of distributions and knowing that $\eta^2(r)''$ is also an even distribution, we get from equation (20) :

$$\tilde{\eta}^2(q) = \frac{S_V}{2q^2} \text{Real}\,(1 - \tilde{G}(q)) \tag{37}$$

with

$$\tilde{G}(q) = \int_{-\infty}^{+\infty} G(r) \exp(iqr)\, dr = \int_0^{+\infty} G(r) \exp(iqr)\, dr\,. \tag{38}$$

The modulus of $\tilde{f}_m(q)$ or $\tilde{f}_p(q)$ ranges between 0 and 1. Looking at the Fourier transform of the rhs of equation (21), we find a converging geometrical series and $\tilde{G}(q)$ reads :

$$\tilde{G}(q) = \frac{\tilde{f}_m(q) + \tilde{f}_p(q) - 2\tilde{f}_m(q)\tilde{f}_p(q)}{1 - \tilde{f}_m(q)\tilde{f}_p(q)} \tag{39}$$

Finally using equations (35), (37) and (39), the small-angle scattering can be written as :

$$I(q) = -\frac{\pi S_V}{q} \frac{d}{dq} \left[\frac{1}{q^2} \text{Real} \left(\frac{(1 - \tilde{f}_m(q))(1 - \tilde{f}_p(q))}{1 - \tilde{f}_m(q)\tilde{f}_p(q)} \right) \right]. \tag{40}$$

The well known Debye expression can be recovered using the chord distribution functions given in equation (8) :

$$I(q) = \frac{8\pi\phi_p(1 - \phi_p)\bar{d}^3}{(1 + \bar{d}^2 q^2)^2} \tag{41}$$

where basic stereology gives two general relations :

$$\frac{1}{\bar{d}} = \frac{1}{\bar{\ell}_m} + \frac{1}{\bar{\ell}_p} \tag{42}$$

and

$$S_V = \frac{4\,\phi_p(1-\phi_p)}{\bar{d}} \tag{43}$$

4. Application to different types of disordered media.

From the experimental point of view, two questions can be raised. First, are the chord distributions efficient to give specific information on the structural disorder ? Second, is the connection with small-angle scattering really described by equation (40) ? In other words, can we find different types of disordered structures where uncorrelation between adjacent chords can be assumed ? Based on the present possibility to make quantitative connections between imaging techniques and small-angle scattering, we critically discuss possible applications to different types of randomness.

4.1 EXPERIMENTAL PROCEDURE AND IMAGE PROCESSING. — For an isotropic and biphasic random medium, the fluctuation autocorrelation function, defined in equation (19), is one of the few characteristics that remain unchanged whether you observe them two- or three-dimensionally [25, 26]. In the following, digitized sections of different porous structures are numerically analyzed. Direct computation of $\eta^2(r)$ is performed along several bundles of parallel lines. These are uniformly distributed along different random directions. To minimize size effect, the maximal value of r is less than 1/3 of the average size of the picture. The small-angle scattering $I(q)$ is computed from equation (35). The chord distribution calculation is performed in four steps : (i) definition of a random direction ; (ii) localization, along this direction, of a pair of nearest neighbor pixels having different values (0 for the pore, 1 for the mass). This pair defines the first end of a chord ; (iii) estimation of the chord segment along the direction chosen. This chord can belong to the pore or to the mass network and (iv) computation of the size histogram by iteration of the former steps. This algorithm gives the chord size distribution in numbers and was checked on basic figures (the cercle for example) where analytical expressions are known. A good agreement is obtained except for the first pixels where the discrete nature of the digital image induces slight artefarcts.

4.2 LONG-RANGE DEBYE RANDOMNESS. — Figure 1 shows a digitized section of dolomite adapted from [27]. The evolution of the pore and the mass chord distributions follows two successive regimes (see Fig. 2). As is the case for a smooth and curved interface, these distributions scale with r at small distances. Just after the maximum of each distribution, a negative exponential form is observed. This is a good example of long-range Debye randomness. In figure 3, we compare the direct computation of $I(q)$ from the image with the chord distribution formalism (Eq. (40)). On the same scale, one observes a good agreement.

4.3 « CORRELATED » DISORDER. — The small-angle scattering of some porous solids shows a peak corresponding to the existence of a relatively well defined correlation length. We discuss how a chord distribution model can succeed or fail to predict the scattering properties of these correlated structures.

Let us first consider the case of a porous glass (Vycor 7930, lot 742098, Trademark Corning). The matrix is prepared by leaching a phase separated borosilicate glass and appears

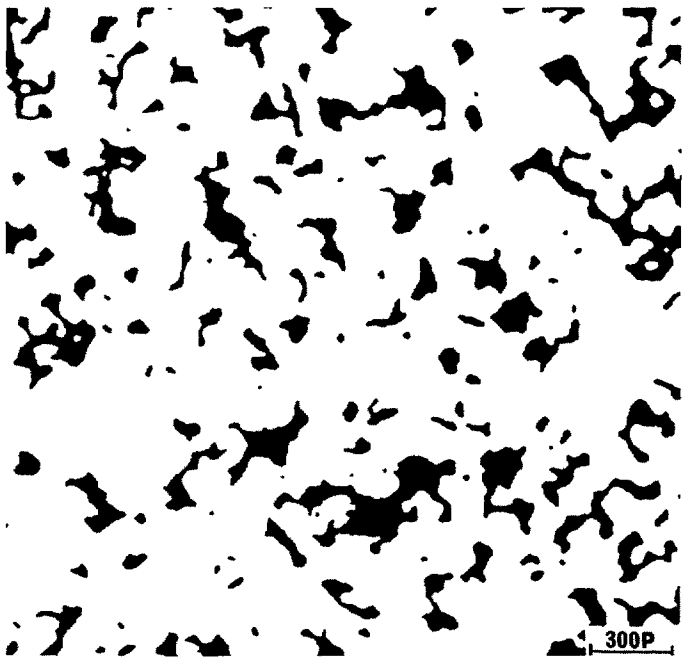

Fig. 1. — Digitized picture of a thin section of dolomite, adapted from reference [27]. The pore network is shown in black. The horizontal bar gives, in pixels, the numerical resolution.

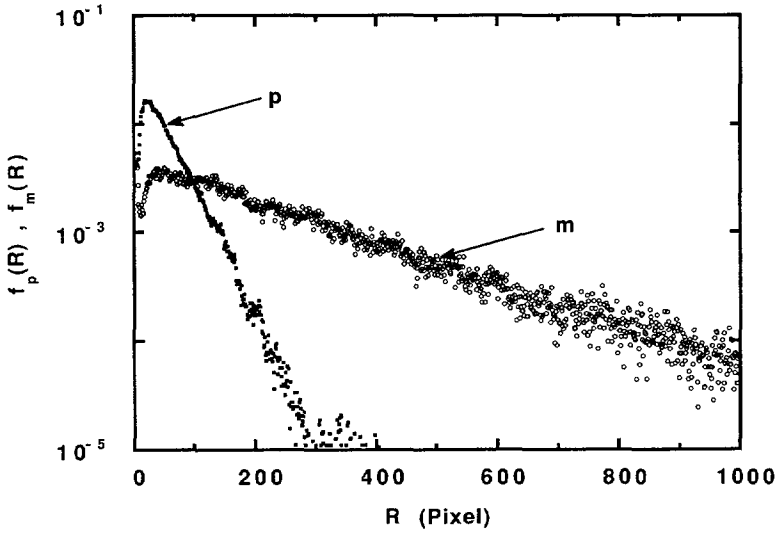

Fig. 2. — Pore and mass chord distribution functions calculated from the digitized image. 1. Full squares : the pore (p) ; Open circles : the solid (m).

as a strongly interconnected and almost pure SiO_2 skeleton. The digitized pore network of a very thin section of this material is shown in figure 4 [3]. The main scattering features of this porous solid is the occurrence of a strong correlation peak around 0.02 $Å^{-1}$ (see Fig. 5)

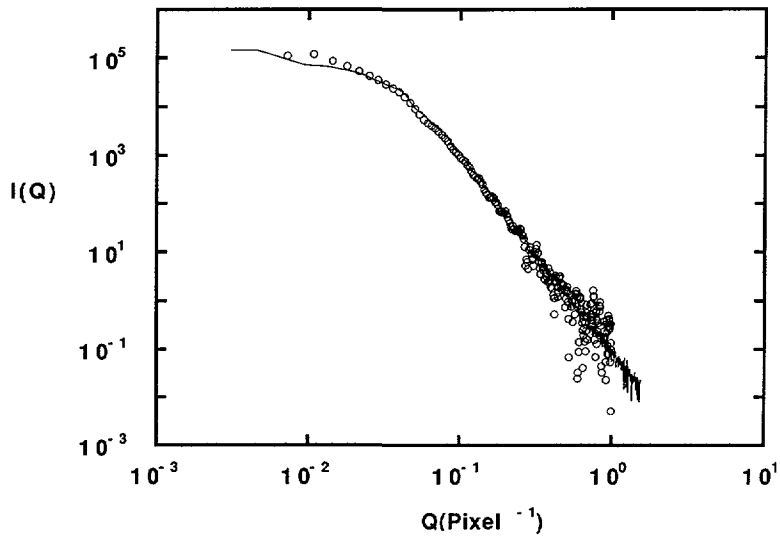

Fig. 3. — Small angle scattering of a porous solid having a random section as the one shown in figure 1. The open circles are the direct computation from the image and the solid line is the calculated scattering using the chord distribution model (Eq. (40)).

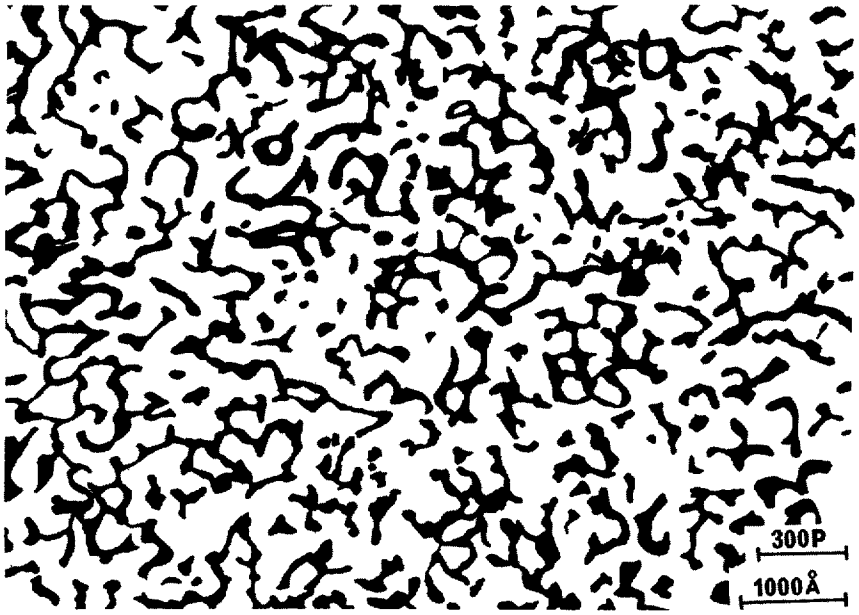

Fig. 4. — Digitized pore network of a very thin section of the porous vycor glass obtained from a transmission electron micrograph [3].

corresponding to a length of 300 Å. The two chord distribution functions are shown in figure 6. A specific mode (a peak) can be observed for each of them, followed by a exponental tail. Computation of the small-angle scattering from equation (40) is in good agreement with a direct estimate using image processing (see Fig. 5). Morover, the « chord distribution » model

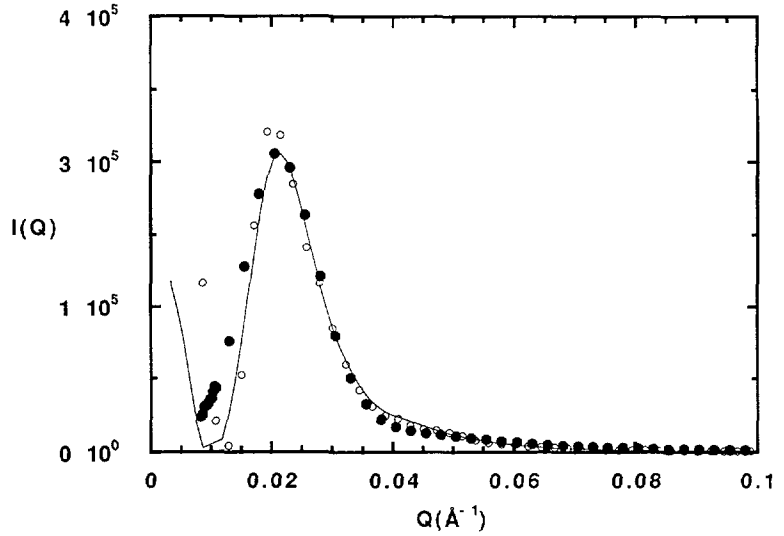

Fig. 5. — Small-angle scattering of the porous vycor glass. The open circles are the direct computation from the image. The solid line is the calculated scattering using the chord distribution model (Eq. (40)). The full circles are the measured small-angle X scattering. This curve is normalized to the calculated scattering using equation (40).

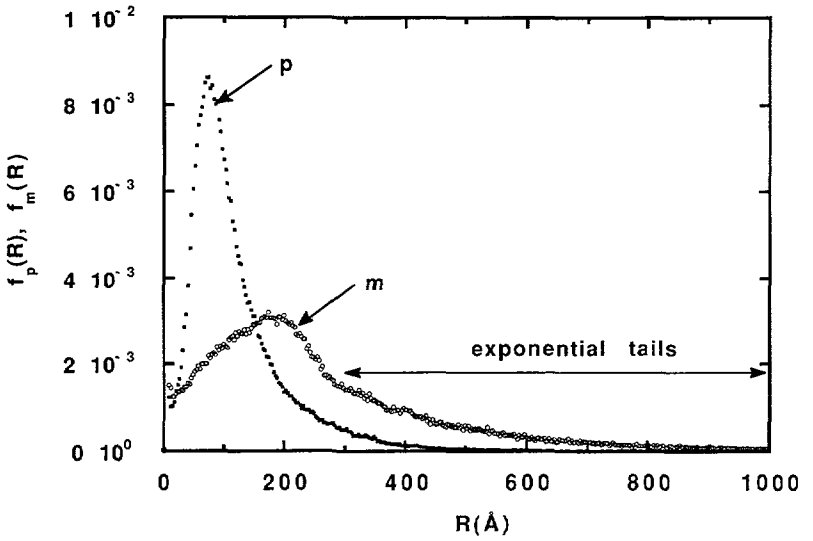

Fig. 6. — Pore and mass chord distribution functions calculated from the digitized image 4 (the porous vycor glass). Full squares : the pore (p) ; Open circles : the solid (m).

fits the experimental correlation peak observed by small-angle X ray scattering. However, two discrepancies can be observed. The model slightly underestimates the left part of the correlation peak and exhibits a q^{-4} dependance in the high q regime (above 0.1 $Å^{-1}$). For this material, the experimental asymptotic behaviour is characterized by a power-law dependence of the form $q^{-3.7}$ The resolution of the digitized pore network, typically 15-20 Å, is in fact too

low to handle possible local roughness of the interface [3]. Nevertheless, the hypothesis concerning the uncorrelation between adjacent chords appears to be acceptable in this « correlated » porous medium.

Another interesting example is displayed in figure 7 showing a thin section of a granular material, built from smooth and almost convex particles. The mass chord distribution exhibits a peak around 100 pixel, followed by an exponential tail (see Fig. 8). The pore distribution

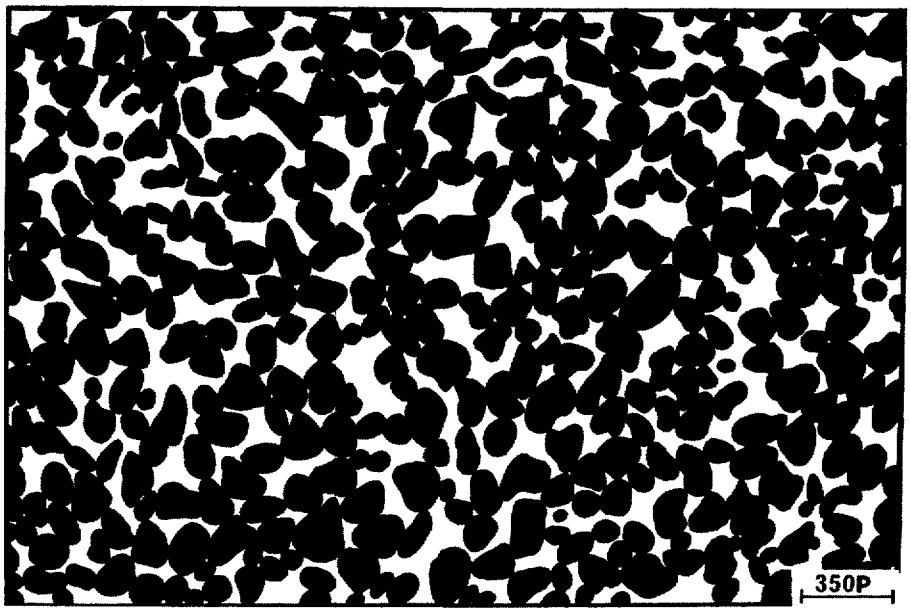

Fig. 7. — Digitized picture of a section of a granular material, adapted from reference [31]. The pore network is shown in white. The horizontal bar gives, in pixels, the numerical resolution.

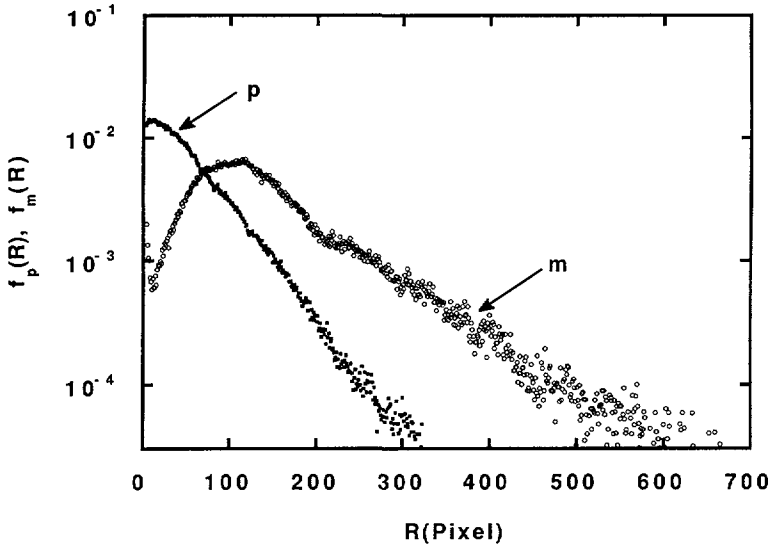

Fig. 8. — Pore and mass chord distribution functions calculated from the digitized image 7 showing a section of a granular porous medium. Full squares : the pore (p) ; Open circles : the solid (m).

continuously decreases from the origin and very rapidly evolves as a negative exponential function. This trend recalls some geometrical properties of a random packing of identical hard spheres. It is known that such a random system exhibits strong correlations spreading on several shells of coordination. Morover the pore chord distribution is shown to have an exponential form [28, 29]. In figure 9, we compare the direct computation of $I(q)$ from the image with the chord distribution formalism (Eq. (40)). The chord model does not fit the scattering curve correctly and gives negatives values at small q ! This example shows clearly the limitation of the chord distributions in predicting the small-angle scattering of a strongly correlated system.

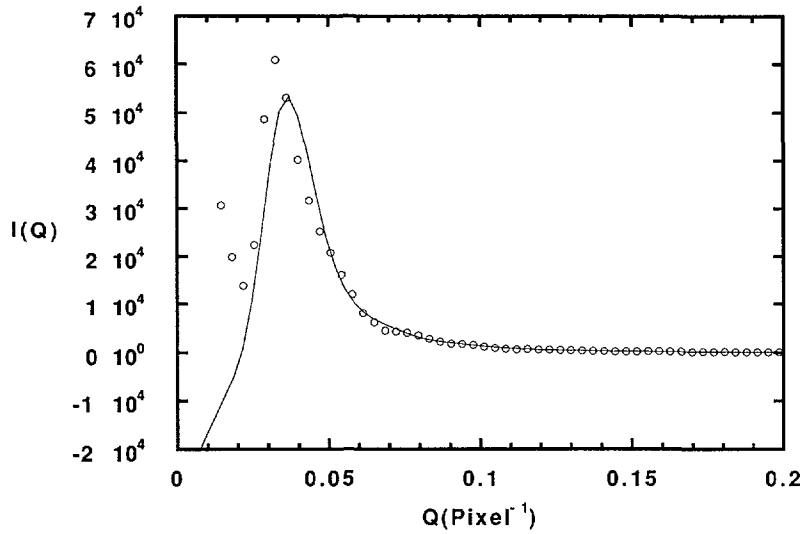

Fig. 9. — Small angle scattering of a porous solid having a random section as that shown in figure 7. The open circles are the direct computation from the image and the solid line is the calculated scattering using the chord distribution model (Eq. (40)).

4.4 COMPLEX STRUCTURES WITH LENGTH SCALE INVARIANCE. — Let us first consider the bidimensional structure shown in figure 10 and known as the diffusion limited aggregate [24, 30]. This is a mass fractal having a fractal dimension of 1.7. The mass chord distribution shows a maximum followed by an exponential tail (see Fig. 11A). At large distances, the pore chord distribution exhibits a $1/q^{\alpha}$ form, with α between 1.65 and 1.70 (see Fig. 11B). These results are in a good agreement with analytical expressions and large r expansions of chord distributions of a mass fractal (See Sect. 2 where $d_m - 1$ gives the fractal dimension of the intersection of a 3D mass fractal and a random plane). The DLA shown in figure 10 does not match any bidimensional cut of a 3D matrix. In that sense, we will focus our attention on the bulk autocorrelation function. As shown in figure 12, the chord model fits the function $\eta^2(q)$ which was computed directly from the image. Two distinct parts can be observed : a Porod regime, at high q, running as q^{-2} and a self similar regime, at small q, in a good agreement with the mass fractal dimension of 1.7.

A more complex organization is exhibited in figure 13 where the digitized image of a thin section of cement (Hydrated calcium silicate) is shown [31]. At large distances, the mass and pore chord distributions evolve in a similar way (See Fig. 14) and approximately decrease as $1/r^{1.65}$ The small-angle scattering computed from equation (40) is shown in figure 15. The

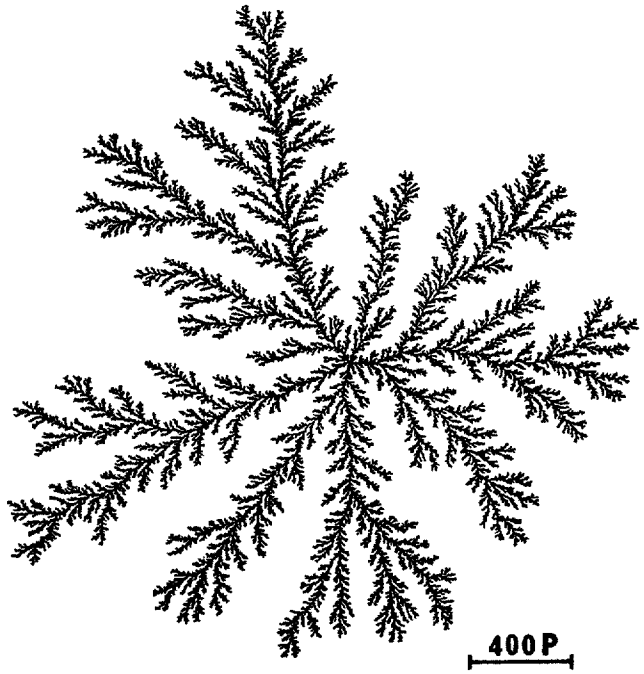

Fig. 10. — Bidimensional DLA adapted from reference [30]. The solid is shown in black. The horizontal bar gives the numerical resolution in pixels.

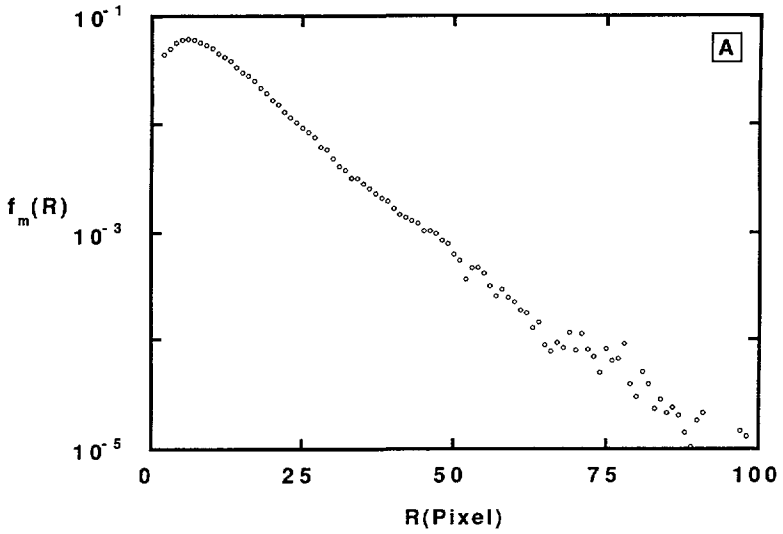

Fig. 11. — A) The mass chord distribution functions calculated from the digitized image 10 (the 2D DLA). B) The pore chord distribution functions calculated from the digitized image 10. The solid line has a slope of – 1.7.

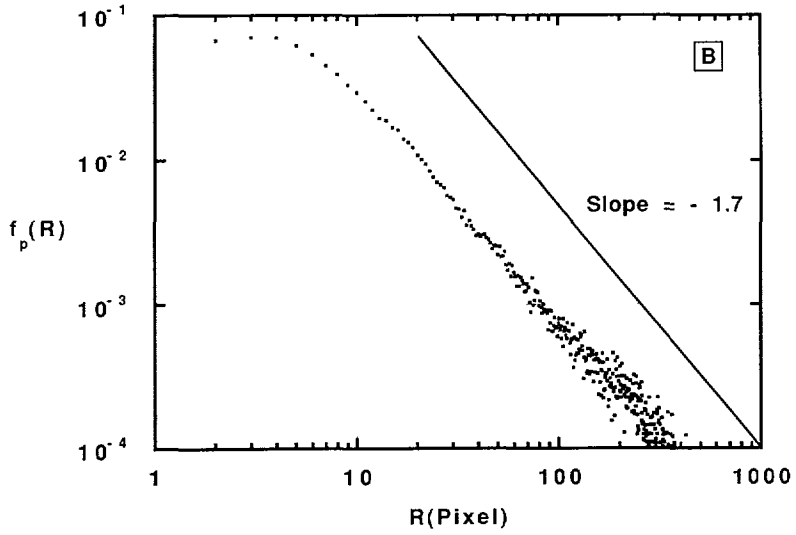

Fig. 11 *(continued).*

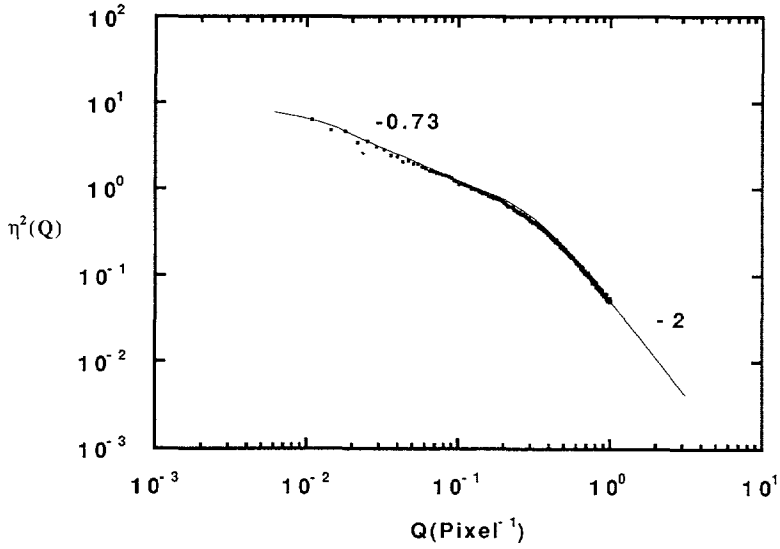

Fig. 12. — Computation of the Fourier transform of the fluctuation autocorrelation function $\eta^2(r)$ in the case of the DLA shown in figure 10. The full squares are the direct computation from the image, using 1D Fourier transform of equation (19). The solid line is the calculated scattering using the chord distribution model (Eq. (37)).

curve scales as $1/q^{3.3}$ for small q and exhibits a Porod law above $q = 0.6$ pixel^{-1} It can be observed that the chord distribution model gives a less noisy result than a direct computation of $I(q)$ from the image. According to the literature [32, 33], the small-angle scattering appears to be related to a surface fractal having a fractal dimension of 2.7. An the other hand, the similar algebraic evolution of the two chord distributions can be described by equation (14) which gives a fractal dimension of 2.65. A different way to check the possibility of a fractal

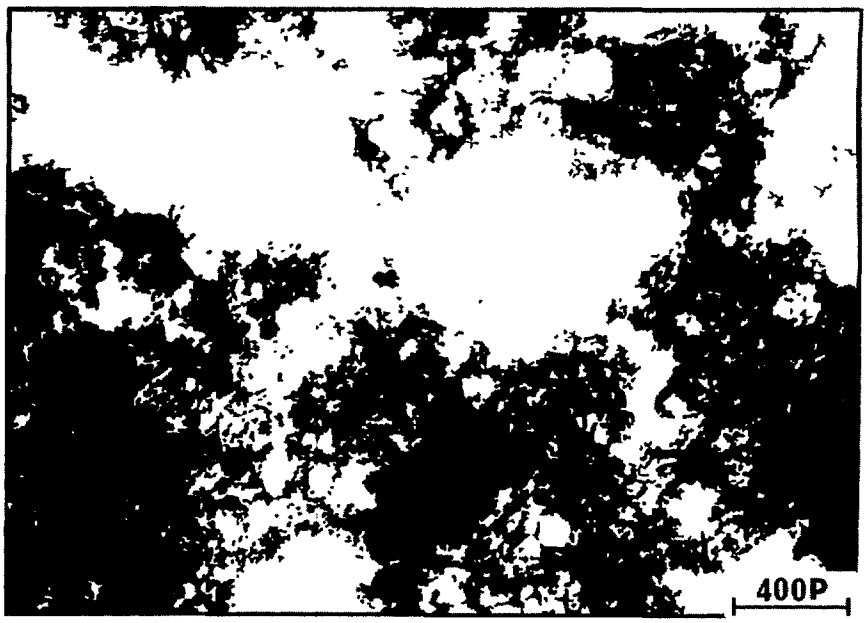

Fig. 13. — Digitized picture of cement, adapted from reference [31]. The pore network is shown in white. The horizontal bar gives the numerical resolution in pixels.

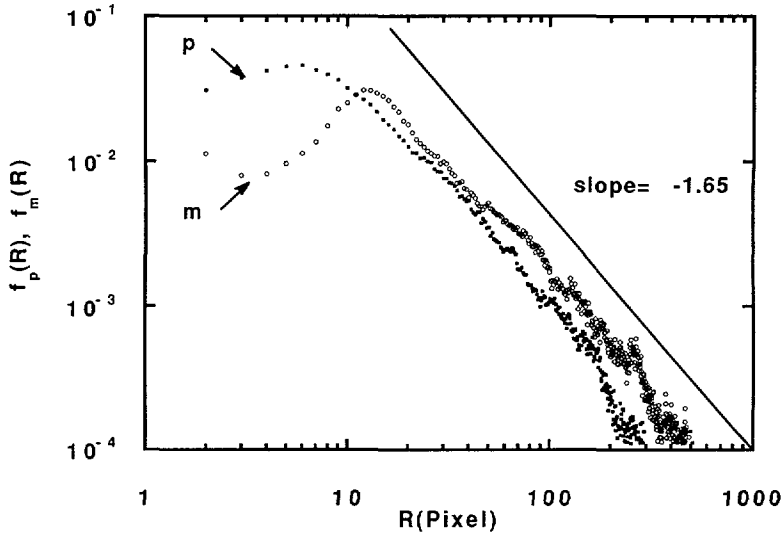

Fig. 14. — Pore and mass chord distribution functions calculated from the digitized image 13. Full squares : the pore (p) ; Open circles : the solid (m).

surface is to analyse the properties of the hull separating the mass and the pore network. On the picture, this interfacial region is defined as the set of pixels belonging to the pore (the mass) network and having one nearest neighbor pixel inside the mass (pore) distribution. This set can be described by using a density which is one in the interfacial region and 0 everywhere else. Figure 16 shows the conditional autocorrelation function of this density. This function

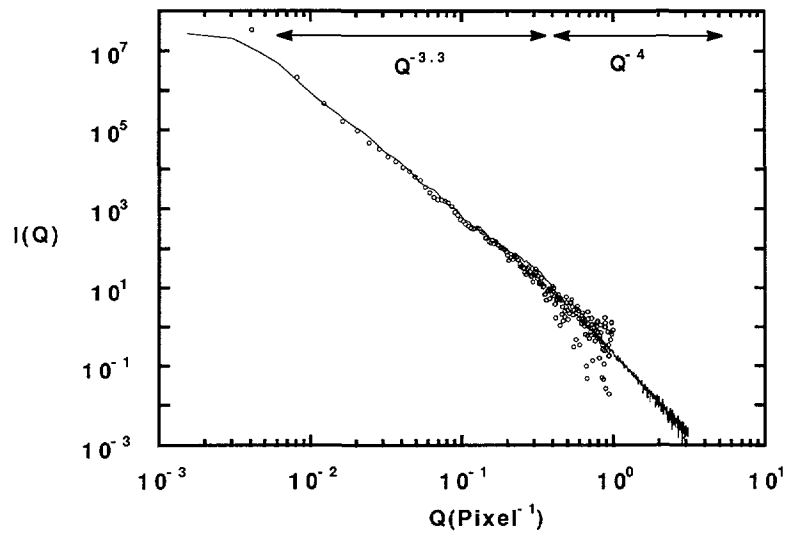

Fig. 15. — Small-angle scattering of a porous solid having a random section as that shown in figure 12. The open circles are the direct computation from the image and the solid line is the calculated scattering using the chord distribution model (Eq. (40)).

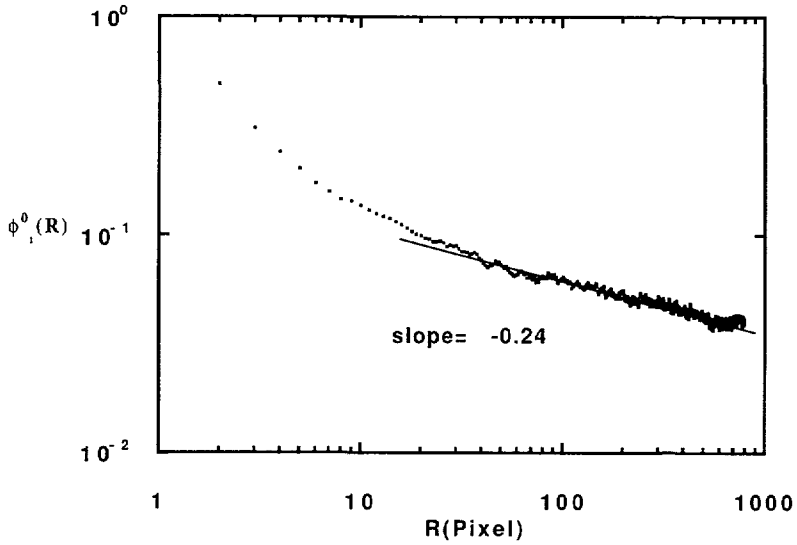

Fig. 16. — « Interfacial » conditional autocorrelation function calculated from the digitized image shown in figure 13 (see text for definition).

gives the average density of interfacial sites at a given distance r of an origin point located inside the interfacial region. At large distances, one observes a $1/r^{0.24}$ dependence related to a fractal dimension (in 3D) of 2.76. This result is in a reasonable agreement with the other two determinations.

5. Conclusion.

The former section shows that the analytic form of chord distribution is sensitive to a specific type of structural disorder. A close inspection of the medium and long-range behaviour of the mass and pore distributions provides a way to distinguish between long range Debye randomness, correlated disorder and mass or surface fractal systems. Computation of small-angle scattering, based on the chord distribution model (Eq. (40)) applies to different types of random binary media. Obviously, equation (40) fails in predicting the scattering of a strongly correlated system where the level of disorder is strongly reduced. The example of porous glass, shown in figure 4, is an interesting intermediate case where correlation and disorder coexist at the mesoscopic scale.

Quantitative connection between imaging techniques and small-angle scattering is very appealing, almost for isotropic systems. This comparison provides a way to clarify different scattering features and to check the likelihood of the image. In this respect, chord distribution functions are not essential but provide enough information to be a valuable structural tool in the elaboration of a reliable and understandable model of disordered porous systems. Application of these distributions is not restricted to small-angle scattering. They play a central role in some transport processes such as direct energy transfer and Knudsen diffusion in a porous medium [3, 34, 35]. In this regard, a direct connection between imaging techniques and small-angle scattering can also be considered as an interesting way to get a reliable description of these chord distribution functions.

Acknowledgments.

Many interesting discussions with J. M. Drake and S. K. Sinha are gratefully acknowledged. The DLA numerical simulation was kindly provided by Peter Ossadnik (Ref. [30]).

References

[1] DULLIEN F. A., Porous Media : Fluid Transport and Pore Structure (Academic Press, 1976).
[2] KLAFTER J. and DRAKE J. M., Molecular Dynamics in restricted Geometries (Wiley Interscience, 1989).
[3] LEVITZ P., EHRET G., SINHA S. K. and DRAKE J. M., *J. Chem. Phys.* **95** (1991) 6151-6161.
[4] AUVRAY L. and AUROY P., Neutrons, X-Ray and Light Scattering, P. Lindner and T. Zemb Eds. (Elsevier Science Publishers, 1991) pp. 199-221.
[5] CICCARIELLO S., COCCO G., BENEDETTI A. and ENZO S., *Phys. Rev. B* **23** (1981) 6474-6485.
[6] KJEMS J. K. and SCHOFIELD P., Scaling phenomena in disordered systems, R. Pynn, A. Skjeltorp Eds. (Plenum Press) *NATO ASI, series B* **123** (1985) 141.
[7] GUINIER A. and FOURNET G., Small angle scattering of X rays (John Wiley & son, 1955) pp. 12-13.
[8] POROD G., Small angle X ray scattering, Syracuse 1965, H. Brumberger Ed. (Gordon and Breach Science Publ., 1967) pp. 1-15.
[9] MERING J. and TCHOUBAR-VALLAT D., *C.R. Acad Sci. Paris* **262** (1966) 1703.
[10] WU H. and SCHMIDT P. W., *J. Appl. Cryst.* **4** (1971) 171-231.
[11] WU H. and SCHMIDT P. W., *J. Appl. Cryst.* **7** (1974) 131-146.
[12] MERING J. and TCHOUBAR D., *J. Appl. Cryst.* **1** (1968) 153-165.
[13] CICCARIELLO S., *J. Appl. Cryst.* **21** (1988) 117-128.
[14] SERRA J., Image analysis and mathematical morphology (Academic Press, 1982) p. 329.
[15] DEBYE P. and BUECHE A. M., *J. Appl. Phys.* **20** (1949) 518-525.

[16] DEBYE P., ANDERSON H. R. and BRUMBERGER H., *J. Appl Phys.* **28** (1957) 679-525.
[17] CICCARIELLO S., *Phys. Rev. B* **28** (1983) 4301-4306.
[18] YAGLOM A. M., Introduction to the theory of stationary random functions (Dover, 1962).
[19] RICE S. O., *Bell System Tech. J.* **23** (1944) 282-332.
[20] LEVITZ P. and TCHOUBAR D., Submitted.
[21] KIRSTE R. and POROD G., *Koll. Z., Z Polym.* **184** (1962) 1-7.
[22] MANDELBROT B. B., The fractal geometry of nature (Freeman, 1982) p. 135.
[23] KOLB M. and HERRMANN H. J., *Phys. Rev. Lett.* **59** (1987) 454-457.
[24] JULLIEN R. and BOTET R., Aggregation and fractal aggregates (World Scientific, 1987).
[25] JOSHI M., Ph. D. thesis, Univ. of Kansas (1974).
[26] QIBLIER J. A., *J. Colloid Interface Sci.* **98** (1984) 84-102.
[27] SCHWARTZ L. M., Dynamic in small confining systems, J. M. Drake, J. Klafter, R. Kopelman Eds., Proceedings of symposium M, Fall meeting of the MRS (1990) pp. 61-63.
[28] DIXMIER M., *J. Phys. France* **39** (1978) 873-895.
[29] PAVLOVITCH A., JULLIEN R. and MEAKIN P., *Physica A* **176** (1991) 206-219.
[30] OSSADNIK P., To appear in *Physica A*.
[31] VAN DAMME H., *Ciments, Bétons, Plâtres, Chaux* **782** (1990) 15-17.
[32] BALE H. D. and SCHMIDT P. W., *Phys. Rev. Lett.* **53** (1984) 596-599.
[33] TEIXEIRA J., On growth and form, H. E. Stanley, N. Ostroswsky Eds. (M. Nijhoff Publishers, 1986) pp. 145-162.
[34] LEVITZ P., in preparation.
[35] DRAKE J. M., LEVITZ P., KLAFTER J., TURRO N. J., NITSCHE K. S. and CASSIDY K. F., *Phys. Rev. Lett.* **61** (1988) 865-868.